JOURNAL OF MATERIALS SCIENCE **40** (2005) 5903–5910

Continuum modeling of strain localization phenomena in metallic foams

S. FOREST*
Ecole des Mines de Paris, CNRS, Centre des Matériaux, UMR 7633, BP 87, 91003 Evry, France
E-mail: samuel.forest@ensmp.fr

J.-S. BLAZY
Centre Technique Renault, Parc de Gaillon, 27940 Aubevoye, France

Y. CHASTEL
Ecole des Mines de Paris, CNRS, Cemef, UMR 7635, 5 rue C. Daunesse, 06904 Sophia–Antipolis, France

F. MOUSSY
Technocentre Renault, 1 avenue du Golf, 78288 Guyancourt, France

Aluminium foams obtained by injecting a gas into the liquid metal are prone to localization of strain and damage. Under compression, crushing bands form, multiply and propagate through the whole sample. A continuum model based on a compressible plasticity framework is presented that is suitable for the simulation of such strain localization bands. The importance of accounting for strain localization phenomena in structural computations is illustrated by finite element simulations of the compression of cube and tapered specimens, and of an indentation test. A regularization procedure is proposed to obtain mesh–independent results.

1. Introduction

Aluminium foams exhibit attractive energy–absorption properties, especially in combination with metal structures. In the case of aluminium foams under compression, the underlying deformation or/and failure mechanism is the localization of strain or/and damage inside thin bands that form, multiply and propagate throughout the whole sample [1]. The intrinsic behaviour of metallic foams cannot be deduced directly from the overall load/displacement curve, as advocated in [2]. Instead, it is essential to take strain localization phenomena into account in the constitutive modelling. Efficient numerical methods are necessary to perform structural computations on engineering components like crash boxes for automotive industry. Accordingly, continuum models are still needed for such applications in order to avoid a detailed description of each individual cell. Simple compressible plasticity models are available, initially developed for powder metallurgy applications or more generally the mechanics of porous media [3]. One of the most simple models, based on a so–called elliptic yield criterion was applied to metallic foams in the references [4–7]. An evaluation of such continuum models for structural computations can be found in [8].

A first attempt to incorporate strain localization effects in such models was proposed in [4] by including explicitly into the constitutive equations the existence of a peak stress followed by a short softening regime systematically observed in the compression curves of aluminium foams. The introduction of softening in a constitutive model leads to possible loss of ellipticity of the set of partial differential equations to be solved in structural computations [9]. It leads to the formation of strain localization bands after the peak stress. This strategy is further developed in the present work and illustrated in the case of structural computations (compression of tapered specimens and indentation). Metallic foams are strongly heterogeneous materials. The inhomogeneous distribution of porosity plays a significant role to trigger strain localization phenomena in foam structures, as already recognized in [10]. This information can be incorporated to simulate more realistic strain localization patterns in aluminium foams. This is done in Section 3.1 in a simple 2D case.

It is well–known that finite element simulations based on strain–softening models are associated with spurious mesh dependence of the results: The finer the mesh, the thinner the strain localization bands [11, 12]. The overall load–displacement curve also is

*Author to whom all correspondence should be addressed.
0022-2461
DOI: 10.1007/s10853-005-5041-6

mesh–dependent. In the case of aluminium, the thickness of strain/damage localization bands is directly related to the size of the cells. In Section 4, an enhanced continuum framework is proposed to include an intrinsic length scale into the model and to obtain mesh–independent simulation results.

Standard index notations are used for tensors throughout the text. The numerical and experimental results given in this work were obtained with an aluminium foam having an overall density of $0.26 \mathrm{g.cm}^{-3}$, which corresponds to an initial porosity $f = 0.90$. It was supplied by Hydro Aluminium [13].

2. Compressible plasticity model for aluminium foams

2.1. Constitutive equations and bifurcation analysis

One of the most simple yield functions for compressible elastoplastic materials is the elliptic potential defined by the following yield function

$$g(\sigma_{ij}) = \sigma_{eq} - R, \quad \sigma_{eq}^2 = \frac{3}{2} C \sigma_{ij}^{\mathrm{dev}} \sigma_{ij}^{\mathrm{dev}} + F(\sigma_{ii})^2 \tag{1}$$

where C and F are material parameters, depending on material porosity f, and R the hardening function. The trace of stress tensor σ_{ij} is given by σ_{ii} with summation over repeated indices. The deviatoric part of the stress tensor is denoted by $\sigma_{ij}^{\mathrm{dev}}$. The tensor giving at each instant the direction of plastic flow $\dot{\varepsilon}_{ij}^{p}$ is

$$N_{ij} = \frac{\partial g}{\partial \sigma_{ij}} = \frac{1}{\sigma_{eq}} \left(\frac{3}{2} C \sigma_{ij}^{\mathrm{dev}} + F(\sigma_{kk}) \delta_{ij} \right),$$
$$\text{and} \quad \dot{\varepsilon}_{ij}^{p} = \dot{p}\, N_{ij} \tag{2}$$

according to the normality rule adopted here for simplicity. δ_{ij} is the Kronecker symbol. The plastic multiplier is $\dot{p}$. The hardening function $R = R_0 + Hp$ (with $R_0 = 200$ MPa and $H = 10$ MPa) corresponds to the estimated intrinsic behaviour of the aluminium composite present in the cell walls. The parameters C and F are explicit functions of the porosity f. These functions are piece–wise linear functions of porosity calibrated from the initial peak stress and following minimal stress level.

In the special case of tension/compression in direction 2, the direction of plastic flow becomes

$$[N] = \frac{\operatorname{sign} \sigma_{22}}{\sqrt{C+F}} \begin{bmatrix} F - \frac{C}{2} & 0 & 0 \\ 0 & C+F & 0 \\ 0 & 0 & F - \frac{C}{2} \end{bmatrix} \tag{3}$$

It can be seen that for $F = 0$, classical von Mises incompressible plasticity is retrieved. The special case $F = C/2$ is associated with no lateral plastic flow in tension/compression. This is a simplification often used for the modeling of the deformation of aluminium foams. One justification is the orientation of strain localization bands obtained for such a value of F predicted in the next paragraph and compared with experimental observations. Values of F different from $C/2$ are found in [5, 7]. They are deduced from the shape of the yield surface under multiaxial loading. However, we will keep this simplified model for the simulation of strain localization phenomena in aluminium foams. These differences suggest that non–associative plasticity models may well be necessary for a complete modeling of deformation and localization modes in metal foams.

The bifurcation analysis performed in [14] and recalled in [12] for general non–associative and compressible elastoplasticity is applied here to the elliptic potential (1). The objective is to determine the orientation of possible strain localization bands that can be deduced from Rice's criterion of loss of ellipticity in elastoplastic solids [9]. Under plane stress conditions, the orientation of the first possible localization band is given by:

$$n_1^2 = \frac{2}{3C} \left(\frac{C}{2} - F \right), \quad n_2^2 = 1 - n_1^2, \quad n_3 = 0 \tag{4}$$

where n_i is the unit vector normal to the strain localization band. If $F = 0$, the classical orientation of shear bands at 55° from the loading axis is recovered (plane stress case). If $F = C/2$, it can be seen that $n_1 = 0, n_2 = 1$. It can be shown that it corresponds to an horizontal strain localization band with an opening mode [12]. This ideal orientation of strain localization bands is in accordance with the quasi–horizontal crushing bands frequently observed in aluminum foams under compression, for instance in [1, 4]. In contrast, more inclined bands usually form in compressed samples of rocks and soils.

2.2. Material parameter identification procedure

The mechanical properties of aluminum foams obtained by injecting gas directly into the liquid metal is investigated in detail in [13]. It turns out that such foams are unable to deform in an homogeneous way during compression. Instead, the short elastic regime is followed by the formation of intense strain localization bands that propagate through the whole specimen. It has already be mentioned that the bands are quasi–horizontal under compressive loading. The formation of the bands is associated with load drops on the overall load/displacement curves and their multiplication and propagation are responsible for the observed plateau. The final stage is densification leading to a sharp increase of the load at the end of the localization process. The horizontal orientation of the bands corresponds to the relation $F = C/2$ between the material parameters involved in the yield function (1).

The formation of the first localization band is associated with an initial peak systematically observed on the overall curve of Fig. 1a. The introduction of this first peak followed by a short softening regime into the constitutive behavior by an appropriate dependency of the parameters C and F on porosity f triggers the

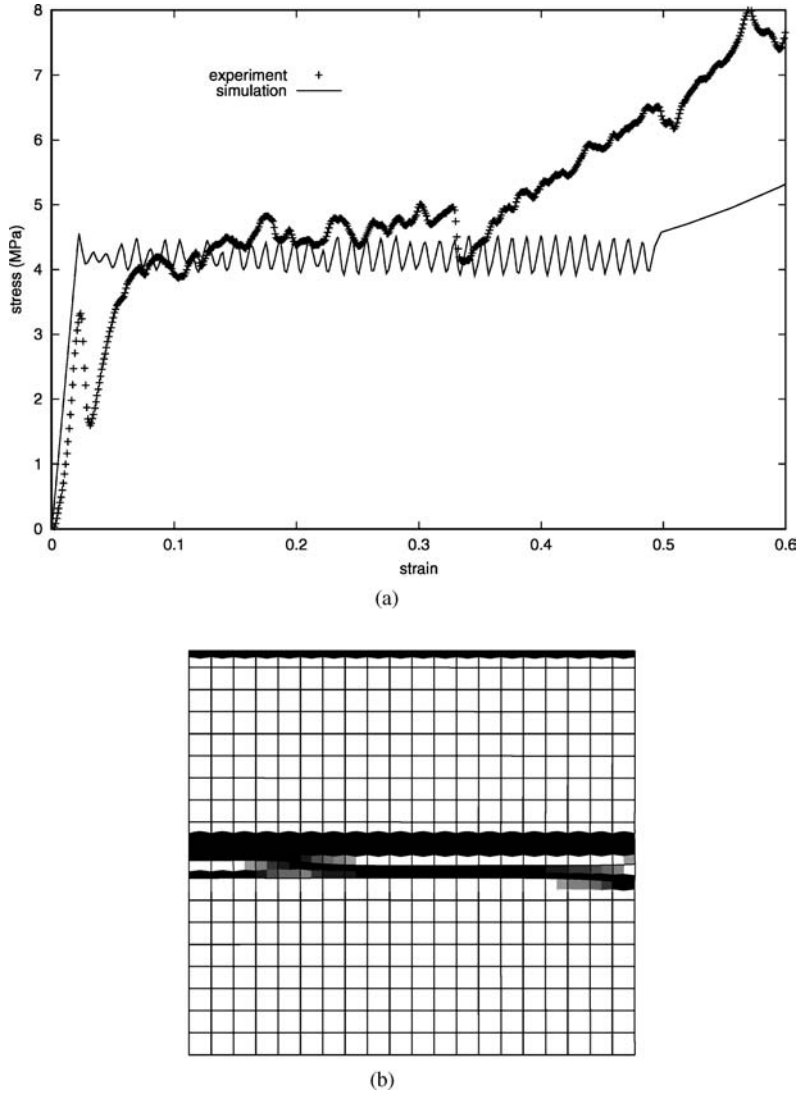

Figure 1 Finite element simulation of the compression of an aluminium foam block: (a) comparison of the computed overall load/displacement curve with experimental results, (b) formation of strain localization bands. The black color corresponds to axial deformation $|\varepsilon_{22}| > 0.55$ and the white color to $|\varepsilon_{22}| < 0.02$.

formation of the first localization band starting from an initial defect of heterogeneity. Densification then takes place inside the band, so that localization will occur again close to the band or at another location. This results in serrations on the simulated overall curve of Fig. 1a. This model was first proposed for metal foams in [4]. The explicit function of the parameters C,F on porosity that makes it possible to incorporate the peak into the constitutive models is reported in [13]. The formation of horizontal crushing bands in a compressed foam block can be seen in the finite element simulation of Fig. 1b. Comparison of the overall load/displacement curve with experimental results on Fig. 1a shows that the model accounts qualitatively for the observed serrations but not for the apparent hardening prior to densification.

3. Simulation of strain localization phenomena in aluminium foams

3.1. Simulation of compression tests starting from 2D tomographic images

Starting from a homogeneous initial porosity field and some initial material imperfections triggering localization, as done in Fig. 1, is not sufficient to account for the slight apparent hardening observed on the experimental load/displacement curve. This is due to the tremendous heterogeneity of the initial porosity field induced by the foaming process, as shown on the view of Fig. 2a obtained by X-ray tomography. The mean cell size is 2.4 mm but the sample contains much smaller and much larger cells. Efficient simulations of components made of aluminum foams require a continuum plasticity model that cannot account for the detailed distribution of large and small cells. Instead, it is proposed to replace the exact aluminum/air distribution by a smeared out porosity field. This is done by attributing to each material point of the image the mean density over a window of given size centered at this point. Such a smeared out porosity field is shown on Fig. 2b and used to initialize the finite element model of Fig. 2c. The size of the averaging box for the local density field is a critical value of the model. It is chosen here such that the porosity range is included in the set of overall porosity values investigated during a large scale campaign of compression tests [13]. It means that for all porosity values on the map of Fig. 2c, we can associate the compression curve of a 100 mm × 100 mm × 100 mm

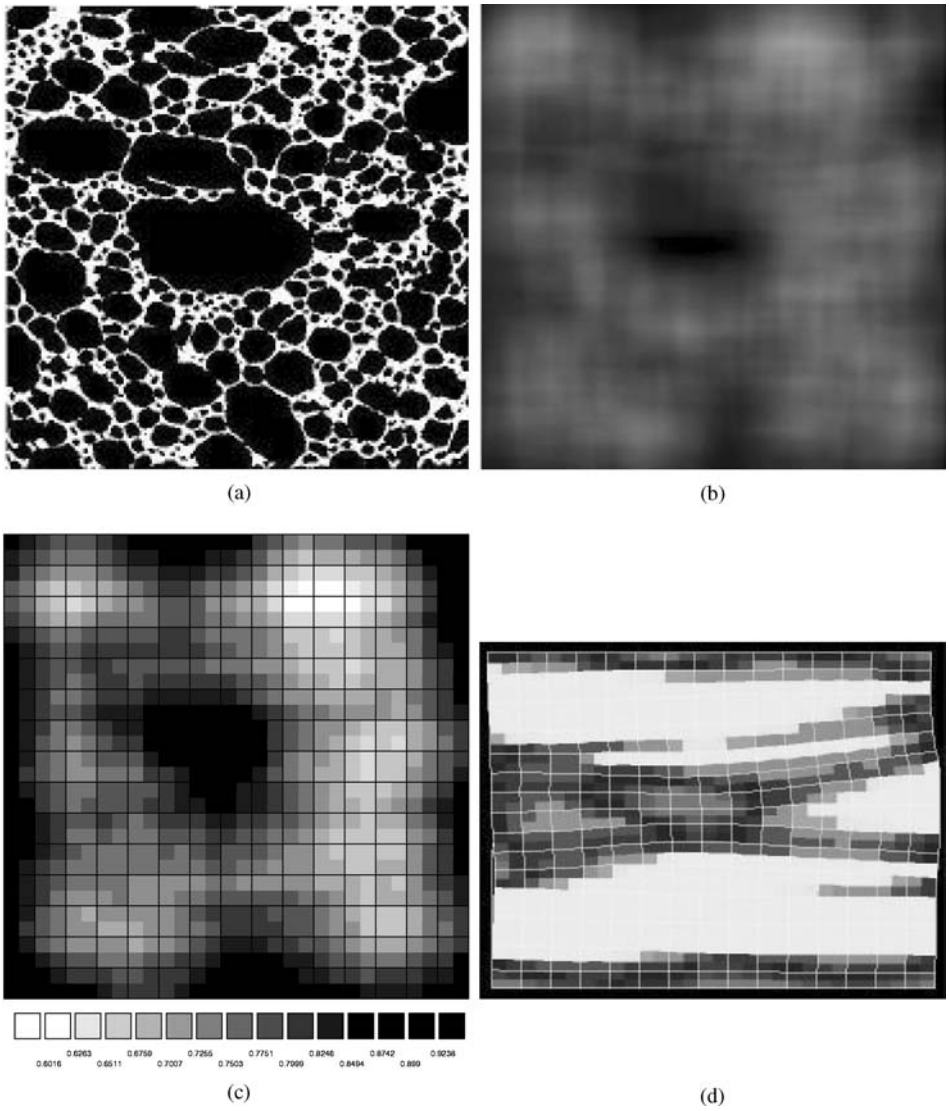

Figure 2 Compression of a slice of aluminium foam: (a) slice extracted from the X-ray tomography of a foam block (image size 50 mm×50 mm), (b) continuous porosity field deduced from the previous image by averaging over a moving window, (c) porosity map in a finite element mesh superimposed on the previous image (the gray scale indicates the porosity range f); axial strain field $|\varepsilon_{22}|$ during compression of the 2D foam block (color scale: white $|\varepsilon_{22}| < 0.1$, black and gray $|\varepsilon_{22}| > 0.5$).

sample having almost the same density. This behaviour is attributed to the corresponding integration point in the finite element analysis, including a function representing the peak stress and subsequent softening. The investigated porosity range is $0.61 < f < 0.98$. The image of Fig. 2a is a square of 398×398 pixels. The chosen averaging domain is 90×90 square and contains therefore about 5×5 cells.

The simulation of the compression of the sample then results in a complex distribution of strain localization bands that correctly mimic the experimental deformation process (Fig. 2). Plastic deformation starts at the large central porosity. The apparent hardening on the overall load/displacement curve is then due to the successive crushing of zones of increasing local density inside the heterogeneous material. A comparison of the local deformation mechanisms with *in situ* X-ray tomography was possible on this sample. The strain localization bands predicted by the model are not located at the same place as the observed ones. This is probably due to the 3D character of the actual deformation of the sample that cannot be accounted for using the present 2D analysis.

The same local averaging procedure was used in [10] in the 3D case for Alulight foams. But there, the simulated strain heterogeneities results only from the heterogeneity of porosity distribution. In our work, strain localization is more severe because of the explicit introduction of strain softening after the initial peak. This gives rise to serrations on the overall curve not accounted for in [10].

3.2. Compression of prismatic samples and indentation

The simulation of such strain localization phenomena is necessary to predict the response of actual components made of metal foams to impacts for instance. This can be illustrated by structural tests and computations. The first one is a compression test on tapered aluminium foam specimens, as proposed in [2]. Finite element simulations of the compression of 75° tapered

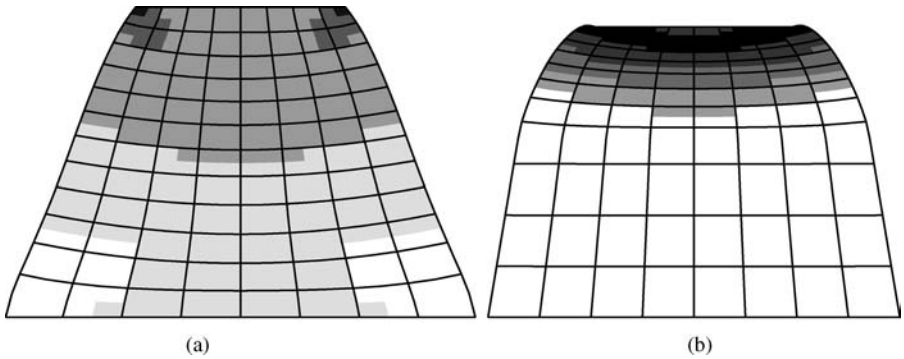

Figure 3 Finite element analyzes of the compression of tapered compression specimens made of aluminium foam: (a) deformed state from a simulation with a compressible plasticity model without taking strain localization into account (white $|\varepsilon_{22}| < 0.02$, black $|\varepsilon_{22}| > 0.3$), (b) deformed state from a simulation of the strain localization zone (white $|\varepsilon_{22}| < 0.02$, black $|\varepsilon_{22}| > 0.5$).

foam blocks were performed with the proposed elliptic model. Two types of simulations are presented. In the first one, the peak stress followed by strain softening is removed from the model. The second type corresponds to the model proposed for the simulation of strain localization, namely that used in Section 2.2, including the peak stress followed by softening. Fig. 3 shows that the plastic zone in the sample is much larger for the first model type (Fig. 3a) than for the second one (Fig. 3b). The latter simulation is in good agreement with the final shape of the sample found experimentally in [2].

Similarly, the size of the plastic zone under a cylindrical indentor is largely overestimated when the indentation process is simulated using an elliptic model that does not take the existence of the peak stress and subsequent softening into account. In contrast, the model proposed in this work predicts a confined and highly deformed plastic zone shown on Fig. 4. Local fracture induced by severe shear at the boundary of the indented surface are not accounted for in the present formulation.

4. Regularization of the compressible plasticity model

In all previous simulations, a fixed finite element mesh size was chosen, approximately equal to twice the mean cell size. The reason is that the thickness of the simulated strain localization bands is always equal to the thickness of one row of integration points (here half an element since each quadratic element contains 4 integration points, cf. Fig. 1a). The mesh dependency of finite element simulations of strain localization phenomena in softening elastoplasticity is well–known [11]. To get rid of this numerical bias, it is necessary to introduce a characteristic length into the constitutive framework. For that purpose strain gradient models have been proposed to handle strain localization phenomena in compressible elastoplastic solids by [15, 16] for instance. A first application to foams was proposed in [17] to model size effects in foam–filled sandwich plates. A similar model based on the so–called micromorphic theory is presented here and applied to the formation of localization bands during the compression of aluminium foams.

4.1. Presentation of the micromorphic foam model

One of the most general higher order continuum is the micromorphic medium that adds to the displacement degrees of freedom u_i a full, non–symmetric, so–called micro–deformation tensor χ_{ij}. The reader is referred to the references [18, 12] for a detailed presentation of the micromorphic continuum. We specialize it here to elliptic elastoplasticity. If χ_{ij} reduces to a pure rotation, the considered material is called a Cosserat medium. In the case of strain localization in cellular solids, the regularizing capabilities of the Cosserat continuum is

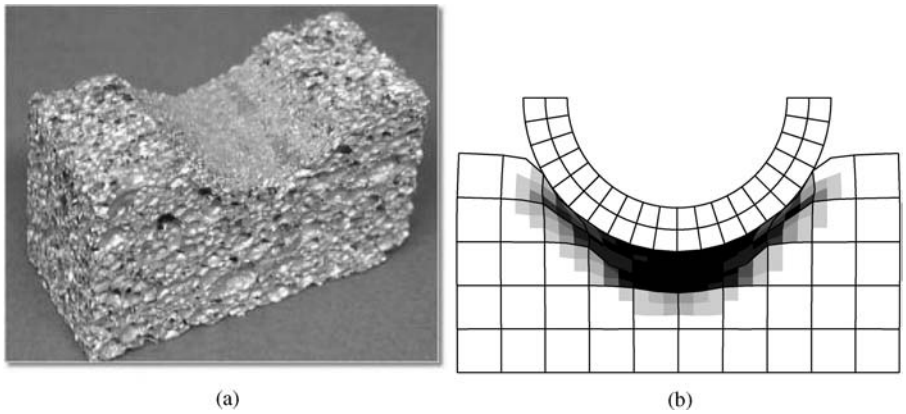

Figure 4 Indentation of a foam block by a rigid cylinder: (a) experiment, (b) finite element simulation taking strain localization under the indentor into account (porosity field: black $f < 0.85$, white $f > 0.90$).

not sufficient because foam deformation is also driven by volume changes not affected by the Cosserat theory. If one introduces the constraint that χ_{ij} be equal to the gradient of the displacement field, the theory reduces to a second gradient model. Three deformation tensors can be defined:

$$\varepsilon_{ij} = \frac{1}{2}(u_{i,j} + u_{j,i}), \quad e_{ij} = u_{i,j} - \chi_{ij}, \quad K_{ijk} = \chi_{ij,k} \tag{5}$$

i.e. the strain, relative deformation and micro–deformation gradient tensors. The comma denotes differentiation with respect to the corresponding coordinate. Three generalized stress tensors must be introduced: the symmetric stress tensor σ_{ij}, the relative stress tensor s_{ij} and a third order stress tensor M_{ijk}. They must fulfill the balance of momentum and balance of moment of momentum equations:

$$(\sigma_{ij} + s_{ij})_{,j} = 0, \quad M_{ijk,k} + s_{ij} = 0 \tag{6}$$

Only the symmetric strain tensor ε_{ij} is split into elastic and plastic parts for the sake of simplicity. The same yield function (1) is kept. The classical constitutive framework presented in Section 2.1 is supplemented by two linear constitutive equations:

$$s_{ij} = 2\alpha e_{ij}, \quad M_{ijk} = A\, K_{ijk} \tag{7}$$

with two additional parameters α and A which must be seen as secant elastoplastic moduli. When it is sufficiently high, parameter α can be regarded as a penalty factor that forces e_{ij} to remain small, i.e. that forces the micromorphic theory to remain close to a second gradient one. Parameter A has the dimension MPa.mm^2. In the next section, it is shown that this parameter is directly related to the thickness of strain localization bands.

4.2. Localization analysis

A micromorphic compressible elastoplastic material is considered, that admits a simple linear softening rule ($H < 0$):

$$R = R_0 + Hp$$

and an elliptic yield function (1). The choice $F = C/2$ (and also a vanishing Poisson ratio to simplify the analytical derivation) ensures that no lateral deformation takes place and that strain localization bands are horizontal according to the standard bifurcation analysis of Section 2.1. The problem becomes actually one–dimensional so that an analytical solution of the localization problem can be worked out for tension/compression along direction 2:

$$\sigma_{eq} = \sqrt{C+F}\,|\sigma_{22}|, \quad \dot{\varepsilon}^p_{22} = \dot{p}\,\sqrt{C+F}, \quad \dot{p} = \frac{2\mu\sqrt{C+F}}{2\mu(C+F)+H}\dot{\varepsilon}_{22} \tag{8}$$

where μ is the shear modulus. For monotonous loading, in the plastic regime, one gets:

$$p = \frac{2\mu\sqrt{C+F}}{2\mu(C+F)+H}\left(\varepsilon_{22} - \frac{R_0}{2\mu\sqrt{C+F}}\right) \tag{9}$$

The balance equations (6) for stresses and the elasticity relations (7) must be taken into account:

$$(\sigma_{22} + s_{22})_{,2} = 0, \quad M_{222,2} + s_{22} = 0$$
$$\sigma_{22} = 2\mu(\varepsilon_{22} - \varepsilon^p_{22}) = \frac{2\mu}{2\mu(C+F)+H}(H\varepsilon_{22} + R_0\sqrt{C+F}), \tag{10}$$
$$s_{22} = 2\mu(\varepsilon_{22} - \chi_{22}), \quad M_{222} = A\chi_{22,2}$$

where $\alpha = \mu$ is assumed for simplicity. A system of equations is obtained for the two unknowns (ε_{22}, χ_{22}):

$$\begin{cases} \bar{H}\varepsilon_{22,2} + 2\mu(\varepsilon_{22,2} - \chi_{22,2}) = 0 \\ A\chi_{22,22} + 2\mu(\varepsilon_{22} - \chi_{22}) = 0 \end{cases}$$
$$\text{where} \quad \bar{H} = 2\mu H/(2\mu(C+F)+H) \tag{11}$$

The micro–deformation χ_{22} is then solution of equation

$$\chi_{22,222} - \frac{2\mu\bar{H}}{A(\bar{H}+2\mu)}\chi_{22,2} = 0 \tag{12}$$

It appears that, when H is negative, the solution is sinusoidal with the wave length:

$$1/\omega = 1/\sqrt{\frac{2\mu|\bar{H}|}{A(\bar{H}+2\mu)}} \tag{13}$$

The strain localization band with indeterminate size predicted by the localization analysis of the classical model is therefore replaced by a strain localization zone of finite width. The localization zone is an arc of sinus curve for this simple model. Additional boundary conditions are necessary to solve actually the differential equations. They concern the components u_i, χ_{ij} or the dual forces $(\sigma_{ij} + s_{ij})n_j$, $S_{ijk}n_k$. In the present case the additional condition $S_{ijk}n_k = 0$ is enforced on lateral free surfaces. At the ends $y = 0, L$ (L height of the block), this condition is used also but it does not have any impact on the solution since the fields are almost homogeneous near these points, so that no micromorphic effect is possible. The micromorphic model was implemented in a finite element program. Fig. 5a shows that mesh refinement leads to a converged deformation zone of finite size. It has the sinusoidal character predicted by the analytical model as shown in Fig. 5b. The details of the implementation are given in [12]. Standard quadratic elements with complete or reduced integration can still be used for this type of continuum. The only difference is the number of degrees of freedom per node: 2 displacement components and 4 components of χ_{ij}, in the two-dimensional case. It is

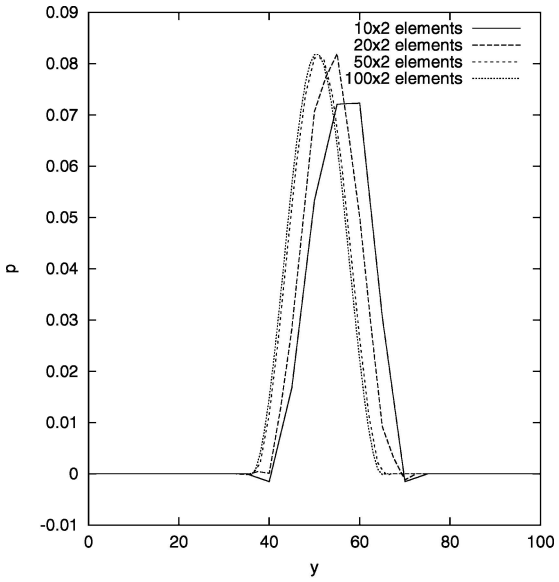

(a)

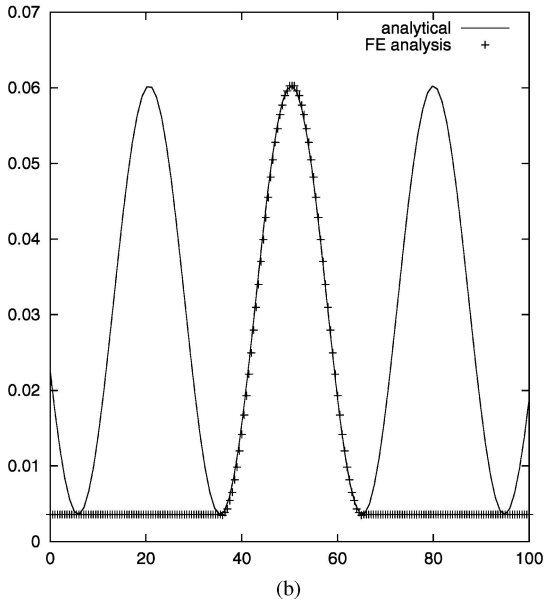

(b)

Figure 5 Finite element analysis of a homogeneous foam block with a central initial defect under uniaxial compression using the micromorphic foam model: (a) influence of mesh refinement on strain localization, (b) comparison between the FE and analytical solutions. The cumulative plastic strain p is plotted against the axial coordinate y.

therefore a good candidate for the regularization of the simulations shown in Section 3.

5. Conclusions

A general continuum framework was presented to simulate strain localization phenomena in aluminium foams based on three main ingredients:

(1) *A compressible plasticity model based on the elliptic potential*. A peak stress followed by a softening regime are introduced in the functional dependence of the material parameters C and F in order to trigger the formation of quasi–horizontal strain localization bands. This model feature leads to the formation, multiplication and propagation of crushing bands in qualitative agreement with experiment. When applied to simple structures like tapered compression specimens and indented blocks, it leads to the development of strongly localized deformation zones as observed experimentally.

(2) *Non homogeneous initial porosity maps, deduced from tomographic images*. Porosity heterogeneities are responsible for the initiation of the first strain bands and for the deviation of propagating bands. Higher local densities lead to an apparent hardening of the overall load/displacement curves.

(3) *A regularization procedure incorporating an intrinsic length scale into the continuum modeling*. A simple micromorphic continuum model was proposed that requires only 2 additional constants. One of them was directly related to the initial thickness of crushing bands. One advantage of the model is the simplicity of its finite element implementation in comparison to other available strain gradient models [19].

Clear relationships between the additional degrees of freedom of the micromorphic foam model and the deformation of individual cells remain to be established. This should be done by comparing 3D X-ray tomography images of available *in situ* tests and full 3D computations with the micromorphic foam model and corresponding continuized porosity maps. In particular, the averaging window size for porosity fields should be carefully related to the introduced intrinsic length scales. Available 3D meshing techniques can now be used to discretize all the heterogeneities present in a given small volume of material analyzed by X-ray tomography, as proposed in [20]. Such unit cell computations can be used to calibrate regularized continuum models, that are necessary for computing larger structures. Other applications of the micromorphic approach to the deformation and fractures of metal foams are proposed in [21].

References

1. H. BART-SMITH, A. F. BASTAWROS, D. R. MUMM, A. G. EVANS, D. J. SYPECK and H. N. G. Wadley, *Acta Metal.* **46** (1998) 3583.
2 T. WIERZBICKI, M. DOYOYO and A. MARKAKI, in, Cellular Metals and Metal Foaming Technology, edited by N. A. Fleck J. Banhart and M. F. Ashby (Verlag MIT Publishing, 2001) p. 449.
3 R. E. MILLER, *Int. J. Mech. Sci.* **42** (2000) 729.
4 Y. CHASTEL, E. HUDRY, S. FOREST and C. PEYTOUR, in, Metal foams and Porous Metal Structures, edited by J. Banhart, M. F. Ashby and N. A. Fleck (Verlag MIT Publishing, 1999) p. 263.
5 V. S. DESHPANDE and N. A. FLECK, *J. Mech. Phy. Solids* **48** (2000) 1253.
6 X. BADICHE, S. FOREST, T. GUIBERT, Y. BIENVENU, J.-D. BARTOUT, P. IENNY, M. CROSET and H. BERNET *Mater. Sci. Enging.* **A289** (2000) 276.
7 J.-S. BLAZY, A. MARIE-LOUISE, S. FOREST, Y. CHASTEL, A. PINEAU, A. AWADE, C. GROLLERON and F. MOUSSY, *Int. J. Mech. Sci.* **46** (2004) 217.
8 A. G. HANSSEN, O. S. HOPPERSTAD, M. LANGSETH, and H. ILSTAD, *ibid.* **44** (2002) 359.
9 J. R. RICE, in Theoretical and Applied Mechanics, edited by W. T. Koiter (North Publishing Company, 1976).
10 B. FOROUGHI, B. KRISZT and H. P. DEGISCHE, in, Cellular Metals and Metal Foaming Technology, edited by N. A. Fleck, J. Banhart and M. F. Ashby (Verlag MIT Publishing, 2001) p. 265.
11 R. DE BORST, L. J. SLUYS, H. B. MÜHLHAUS and J. PAMIN, *Enging. Comp.* **10** (1993) 99.
12 J. BESSON, Local Approach to Fracture (Ecole des Mines de Paris–Les Presses, 2004).

13 J.-S. BLAZY, Comportement mécanique des mousses d'aluminium: Caractérisations Expérimentales Sous Sollicitations Complexes et simulations numériques dans le cadre de l'élasto–plasticité compressible (Doctoral thesis, Ecole des Mines de Paris, 2003).
14 N. S. OTTOSEN and K. RUNESSON, *Int. J. Sol. Stru.* **27** (1991) 401.
15 R. CHAMBON, D. CAILLERIE and T. MATSUCHIMA, *ibid.* **38** (2001) 8503.
16 T. MATSUCHIMA, R. CHAMBON and CAILLERIE, *Int. J. Numer. Meth. Engng.* **54** (2002) 499.
17 C. CHEN and N. A. FLECK, *J. Mech. Phy. Sol.* **50** (2002) 955.
18 S. FOREST and R. SIEVERT, *Acta Mechanica.* **160** (2003) 71.
19 J. Y. SHU, W. E. KING and N. A. FLECK, *Int. J. Numer. Meth. Engng.* **44** (1999) 373.
20 E. MAIRE, A. FAZÉKAS, L. SALVO, R. DENDIEVEL, Y. SOUHAIL, P. CLOETENS and J. M. LETANG, *Comp. Sci. Technol.* **63** (2003) 2431.
21 T. DILLARD, Comportement mécanique et rupture des mousses de nickel : caractérisation 3D, mesures de champs et simulation numérique (Doctoral thesis, Ecole des Mines de Paris, 2004).

Received December 2004
and accepted April 2005